CONNECTING ATOMISTIC-TO-CONTINUUM COUPLING AND DOMAIN DECOMPOSITION

MICHAEL L. PARKS†, PAVEL B. BOCHEV†, AND RICHARD B. LEHOUCQ†

Abstract. Many atomistic/continuum coupling algorithms utilize an overlapping subdomain method, where boundary data for local solves in atomistic and discretized continuum subdomains is provided from local solves in neighboring subdomains. Such coupling algorithms are closely related to the classical alternating Schwarz domain decomposition method, although little to no convergence or error analysis exists for such methods in an atomistic/continuum framework. We consider a specific alternating Schwarz algorithm for coupling a nonlocal atomistic model with a local finite element model and carry out a convergence and error analysis along with supporting numerical experiments.

Key words. Atomistic-to-Continuum, Alternating Schwarz, Lattice statics.

AMS subject classifications. 65N30, 65F10, 74G45, 82D25

1. Introduction. Atomistic/continuum coupling methods are motivated by the desire to study material domains on scales where atomistic effects are important but fully atomistic simulation is not feasible. Such coupling schemes call for decomposition of the material domain into atomistic and continuum subdomains, where the continuum subdomain is modeled via a finite element analysis. The treatment of the interface between these subdomains, or "handshake region", is primarily what distinguishes one atomistic/continuum coupling method from another. In this transition region, approximations are made such as treating finite element nodes as atoms, or vice-versa, to accommodate the incompatibility between a non-local atomistic description and a local finite element description.

A complete theory of this transition region does not yet exist. However, the atomistic-to-continuum coupling problem has similarities with the classical continuum-to-continuum domain decomposition problem. We will explore some of these similarities and address the extent to which both problems can be placed within the same mathematical and algorithmic framework. We focus only on analysis of methods to couple length scales (statics). Analysis of the many schemes proposed to couple length and time scales (dynamics) is a separate but related problem requiring additional analysis.

Many different approaches to couple atomistic and continuum domains have been proposed; see any of the reviews [28, 8, 24, 36, 12]. In general, little mathematical analysis exists for the many proposed coupling methods. However, for the quasi-continuum (QC) method [34, 25], a well-known technique for coupling atomistic and discretized continuum domains in the static (zero temperature) case, some analysis has been accomplished [16, 22, 4, 23, 10].

To deal with the local/nonlocal interface in the transition region, the QC method approximates the global atomic energy functional in the continuum region and the transition region. This has the attractive feature that a single global energy functional is generated with far fewer degrees of freedom than the corresponding global atomistic model. Unfortunately, to the extent that these approximations are inexact, so-called "ghost forces" are generated and must be explicitly corrected [31]. In general, any

†Sandia National Laboratories, Computational Mathematics and Algorithms, P.O. Box 5800, MS 1320, Albuquerque NM 87185 (mlparks@sandia.gov, pbboche@sandia.gov, rblehou@sandia.gov). Sandia is a multiprogram laboratory operated by Sandia Corporation, a Lockheed Martin Company, for the United States Department of Energy under contract DE-AC04-94-AL85000.

coupling approach that generates a well-defined global energy functional must sacrifice accuracy [8]. Many other atomistic/continuum coupling algorithms avoid this issue altogether by taking an alternative approach to the coupling problem. Utilizing overlapping subdomains, they perform a solve on the atomistic subdomain, thus generating boundary conditions for the continuum domain, then perform a solve on the continuum domain, thus generating boundary conditions for the atomistic domain, and repeat until convergence. Subdomain solves require only local energy functionals for the atomistic and continuum domains, and thus a global energy functional is never needed. This type of "back-and-forth" iteration process is employed by methods for many different atomistic/continuum coupling problems, including the FEAt method [17], as well as the coupling schemes proposed by Li et al [19, 20, 21], Hadjiconstantinou [14, 15, 38], Werder et al [37], Tang and Aluru [35], and Nie et al [26, 27].

This process of back-and-forth iteration between domains is known as *alternating Schwarz* [30] within the domain decomposition community, and is generally regarded as the original domain decomposition method. For more on this method, see [32, 29]. Although others such as Hadjiconstantinou [14, 15, 38] have recognized that specific atomistic/continuum coupling schemes are essentially alternating Schwarz, no error or convergence analysis exists.

In section 2 we introduce a prototypical atomistic/continuum model and define a specific atomistic/continuum alternating Schwarz coupling algorithm. In section 3 we perform error and convergence analyses on this algorithm. We demonstrate conditions under which the atomistic solution will be recovered. We conduct numerical experiments supporting our analysis in section 4, and offer conclusions in section 5.

2. A Prototypical Atomistic/Continuum Model. We begin by defining a global atomistic domain of finite extent, which will consist of a one, two, or three-dimensional Bravais-like lattice of atoms. A sample two-dimensional lattice is shown in Figure 2.1(a). We suppose that all atoms share a bond with their r^{th} nearest neighbors ($r \geq 1$) where each bond is represented by a linear spring, to define a mass-spring network. That is, $r = 1$ implies all particles are connected to their nearest neighbors, $r = 2$ implies all particles are connected to their nearest and second-nearest neighbors, etc. We define a corresponding one, two, or three-dimensional global finite element domain where the finite element nodes are located at the lattice sites. A sample two-dimensional finite element domain is shown in Figure 2.1(b). For our finite element model, we assume piecewise linear finite element shape functions.

We consider a global finite element model with nodes located at lattice sites only for ease of presentation, as such a model does not reduce the total number of degrees of freedom and thus presents no computational savings over the corresponding global atomistic model. In general, an atomistic domain is coupled with a finite element mesh more coarse than the atomic lattice. In such a coupling, atomistic positions are computed by evaluating the displacement fields of the finite element solution at the undeformed atom position. Likewise, finite element nodal displacements are computed by evaluating the local atomic displacement field in the region around the undeformed nodal position. For ease of presentation, we omit these grid-transfer operators from our analysis.

For simplicity, we assume that we are modeling a homogeneous linear elastic material with some tensile elastic modulus E. Clearly, our global atomistic and finite element models are simply two different descriptions of the same physical material, and we desire that they both permit certain solutions, such as recovering a constant strain under an applied constant stress. In general, we desire that all Cauchy-Born

deformations [6, 11] be recovered exactly by the coupled model. The theory to be presented is general in that it does not require that we couple only homogeneous materials, and holds for any mass-spring network coupled to any corresponding FEM model.

We briefly describe a mathematical relationship between any atomistic and discretized continuum models we might wish to couple, and show their connections in Figure 2.2. Upscaling our atomistic model via an appropriate limit process will recover an associated continuum PDE. There are many examples of this limiting process. Berezhnyy and Berlyand showed sufficient conditions on a mass-spring network such that it admits a continuum limit [2]. Blanc et al [5] showed how to write certain continuum mechanical models as an asymptotic limit of molecular models. In [9], E and Huang upscale a Frenkel-Kontorova model to recover the Klein-Gordon equation. Further, Arndt and Griebel show how to recover continuum mechanical models from atomistic models for crystalline solids [1]. Likewise, if our atomistic model is a regular mass-spring network, we may view it as a finite-difference discretization of our PDE. However, the atomistic model is not generally directly recoverable from the PDE.

Referring again to Figure 2.2, we see that a finite element discretization of the continuum PDE produces our finite element model, and the PDE can be recovered from that model in the limit where the mesh spacing h goes to zero [7]. Note that our finite element model can then be derived from our atomistic model by first upscaling our atomistic model and then applying the method of finite elements to the resulting PDE. In general, we may use any acceptable discretization of our continuum equations. It is important to note that we have gone from a *nonlocal* atomistic model to a *local* finite element model. Interatomic potentials for an atomistic model describing real materials effectively span over many atoms, and are thus nonlocal. Common finite element shape functions have local support, meaning that the functions associated with a given node are nonzero only in elements associated with that node, and thus the displacement of any point within an element depends only on the displacements of the nodes of that element. For a more detailed discussion of the differences between local and nonlocal models, see [8]. This local-nonlocal coupling will become the primary focus of our later analysis.

We note here that the name *atomistic/continuum coupling* is a misnomer. We never couple an atomistic model to a continuum model, but only to a discretized continuum model, such as a finite element model.

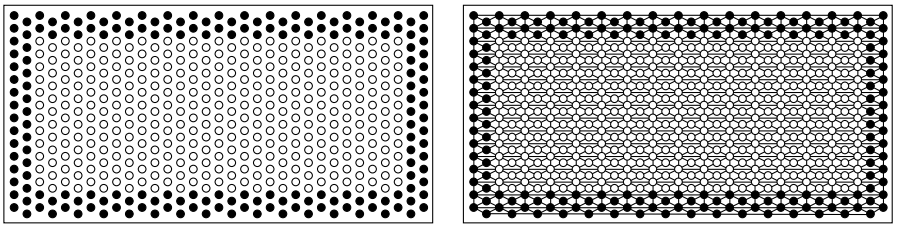

(a) Example atomic lattice.

(b) Example finite element mesh with triangular elements.

FIG. 2.1. *Example two-dimensional atomic lattice and associated finite element mesh derived from lattice nodes. Dark atoms/nodes are taken to be fixed-displacement (Dirichlet) boundary atoms/nodes.*

We now describe the specific coupled atomistic/finite element model that we will

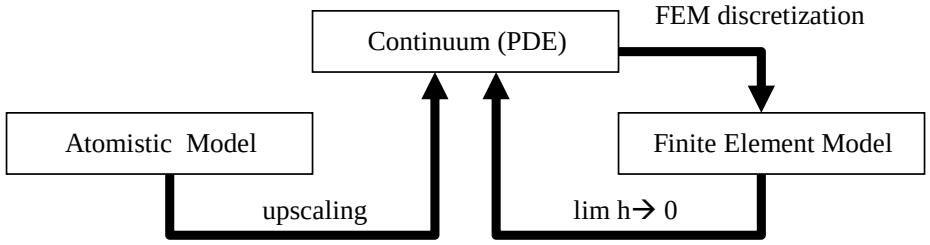

FIG. 2.2. *Mathematical relationships between three related models. Upscaling of the (nonlocal) atomistic model will recover a continuum PDE. A finite element discretization of that PDE will produce a (local) finite element model.*

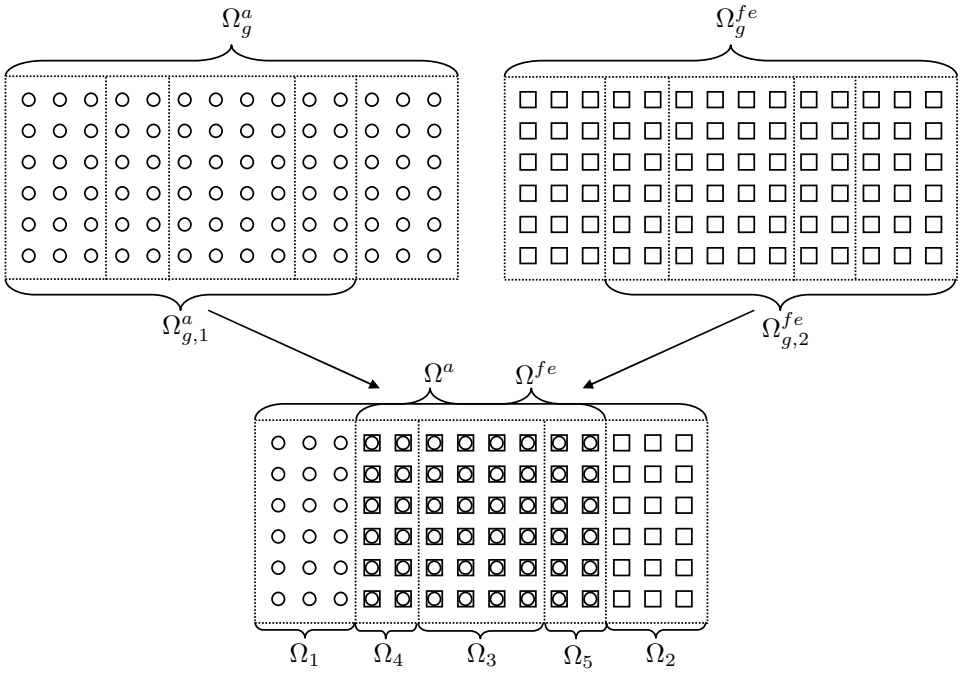

FIG. 2.3. *Construction of a coupled model by overlapping subdomains of atomistic and finite element models. Circles represent atoms, and squares finite element nodes. Both are present in the overlap region of the coupled model.*

analyze. Denote the global atomistic domain by Ω_g^a and the global finite element domain by Ω_g^{fe}, such as those depicted in Figure 2.3. We can define corresponding overlapping subdomains on each global model, which we denote as $\Omega_{g,1}^a$, $\Omega_{g,2}^a$, $\Omega_{g,1}^{fe}$, and $\Omega_{g,2}^{fe}$. Now construct a coupled atomistic/finite element model using $\Omega_{g,1}^a$ from the global atomistic model and $\Omega_{g,2}^{fe}$ from the global finite element model, as depicted in Figure 2.3 for a simple 2D case. As our primary focus in this paper is on the coupled model, we will simplify our notation by henceforth referring to the atomistic subdomain *in the coupled model* as Ω^a and the finite element subdomain *in the coupled model* as Ω^{fe}. We can use these domain boundaries to define five non-overlapping subdomains in the coupled model, which we will call $\Omega_1, \ldots, \Omega_5$. By definition, we have that $\Omega^a = \Omega_1 \cup \Omega_4 \cup \Omega_3 \cup \Omega_5$ and $\Omega^{fe} = \Omega_4 \cup \Omega_3 \cup \Omega_5 \cup \Omega_2$. Without loss of

generality, suppose that the degrees of freedom in Ω_1 are numbered first, those in Ω_2 second, and so on. Additionally, suppose that the degree-of-freedom numberings in the global atomistic and global finite element models matches that of the coupled model.

When performing a solve in the atomistic subdomain Ω^a, the atoms in subdomain Ω_5 will be held fixed. Correspondingly, in the finite element subdomain Ω^{fe}, the finite element nodes in subdomain Ω_4 are subject to a Dirichlet boundary condition. The size of the subdomain Ω_3 can be altered to control the size of the subdomain overlap. Because the finite element model is a local model, the domain Ω_4 need only be a surface (in 3D) or a line (in 2D), but the domain Ω_5 must be at least equal to the cutoff radius used in the atomic model. This is to "saturate" the bonds of the atoms in domain Ω_3 (and also possibly or Ω_4 or Ω_1), and thus prevent these atoms from acting as if they are in the presence of a surface. The subdomain boundaries in the coupled model are artificial, should never produce surface effects.

Having defined a global atomistic model, a global finite element model, and coupled model, we now describe the specific alternating Schwarz algorithm we will analyze in the next section.

Algorithm 1 Atomistic/Continuum Schwarz

1: Initialize displacements of all non-Dirichlet finite element nodes in Ω^{fe}.
2: Initialize positions of all non-fixed atoms in Ω^a.
3: **while** not converged **do**
4: Fix positions of atoms in domain Ω_5 according to positions of finite element nodes in Ω_5.
5: Solve for displacements of unconstrained atoms in atomistic subdomain Ω^a.
6: Fix displacements of finite element nodes in Ω_4 according to positions of atoms in Ω_4.
7: Solve for displacements of unconstrained finite element nodes in Ω^{fe}.
8: **end while**

Because we do not define a global energy functional, we cannot compute a global residual for our coupled model. Further, if we do define and minimize a global energy functional, our model will be subject to ghost forces, as discussed earlier. Instead, we say that our atomistic/continuum Schwarz algorithm has converged if the relative change in the global solution vector is less than some tolerance ε. The well-known limitation in this convergence test is that it may report convergence prematurely if the algorithm is converging slowly. As we will see later, we have some control over the convergence rate of the algorithm and can avoid this problem in practice. In particular, we will see that the rate of convergence increases with the size of the subdomain overlap.

3. Error and Convergence Analysis. From the global atomistic and finite element models described above, let us write down the corresponding stiffness matrices and force vectors. For the global atomistic model (corresponding to Figure 2.1(a), for example), we have

$$K_g^a u_g^a = f_g^a, \tag{3.1}$$

and for the global finite element model (corresponding to Figure 2.1(b), for example) we have

$$K_g^{fe} u_g^{fe} = f_g^{fe}, \tag{3.2}$$

where $K_g^a, K_g^{fe} \in \mathbb{R}^{n\times n}$, and $u_g^a, u_g^c, f_g^a, f_g^{fe} \in \mathbb{R}^n$, where n is the number of unconstrained degrees of freedom in the respective global models. Additionally, let there be n_i unconstrained degrees of freedom in domain Ω_i $i = 1, \ldots, 5$, with respect to the global models, such that $n = n_1 + n_2 + n_3 + n_4 + n_5$.

Here, u_g^{fe} is the solution of the global finite element model, and u_g^a is the solution of the global atomistic model. In the atomistic model, we clearly can only apply forces to atoms. In our continuum (PDE) model, we can apply body and surface forces, but after a finite element discretization, these forces are realized as nodal forces.

For clarity, we explain the details of the alternating Schwarz domain decomposition method here. As is well known, the classical alternating Schwarz algorithm can be recast as a projection method [29]. To assist our analysis, we begin by recasting algorithm 1 as a projection method. Let us define the operators R_1 and R_2 such that the stiffness matrix associated with subdomain Ω^a in our coupled model (see Figure 2.3) can be written as

$$K^a = R_1^T K_g^a R_1,$$

and the stiffness matrix for the finite element subdomain Ω_{fe} in our coupled problem (see Figure 2.3) can be written as

$$K^{fe} = R_2^T K_g^{fe} R_2.$$

Here, $R_1 \in \mathbb{R}^{n\times(n_1+n_4+n_3)}$ and $R_2 \in \mathbb{R}^{n\times(n_3+n_5+n_2)}$ are extension operators, and R_1^T and R_2^T are the corresponding restriction operators. Given the atom / node numberings we have defined, they can be written as

$$R_1 = \begin{bmatrix} I & 0 & 0 \\ 0 & 0 & 0 \\ 0 & I & 0 \\ 0 & 0 & I \\ 0 & 0 & 0 \end{bmatrix}, \qquad R_2 = \begin{bmatrix} 0 & 0 & 0 \\ I & 0 & 0 \\ 0 & I & 0 \\ 0 & 0 & 0 \\ 0 & 0 & I \end{bmatrix},$$

where I represents an identity matrix of appropriate dimension, and 0 a zero matrix of appropriate dimension. We may then rewrite the core of algorithm 1 as the following two steps:

$$\begin{aligned} u_{k+1/2} &= u_k + R_1 (K^a)^{-1} R_1^T (f_g^a - K_g^a u_k), \\ u_{k+1} &= u_{k+1/2} + R_2 (K^{fe})^{-1} R_2^T (f_g^{fe} - K_g^{fe} u_{k+1/2}), \end{aligned}$$

where u_k is the solution to the coupled problem at iteration k, and u_0 is initialized in steps 1 and 2 of algorithm 1. Substituting in (3.1) and (3.2) gives

$$\begin{array}{ll} u_{k+1/2} & = u_k + R_1 (K^a)^{-1} R_1^T K_g^a (u_g^a - u_k) \qquad\qquad = u_k + P^a \left(u_g^a - u_k \right), \\ u_{k+1} & = u_{k+1/2} + R_2 (K^{fe})^{-1} R_2^T K_g^{fe} (u_g^{fe} - u_{k+1/2}) \quad = u_{k+1/2} + P^{fe} \left(u_g^{fe} - u_{k+1/2} \right), \end{array}$$

where $P^a \equiv R_1 (K^a)^{-1} R_1^T K_g^a$ and $P^{fe} \equiv R_2 (K^{fe})^{-1} R_2^T K_g^{fe}$ are projection matrices. In particular, P^a is a K_g^a-orthogonal projector onto the space $\mathcal{R}(R_1)$, and P^{fe} is a K_g^{fe}-orthogonal projector onto the space $\mathcal{R}(R_2)$, where $\mathcal{R}$ denotes the range of a matrix.

We are interested in conditions for which our coupled model recovers the global atomistic solution u_g^a. To that end, we define the error at step k with respect to the

global atomistic solution as $e_k^a \equiv u_k - u_g^a$. Further, we define the vector d such that $u_g^{fe} = u_g^a + d$. That is, d may be viewed as the difference of the global finite element and global atomistic solutions.

Combining the two-step algorithm above into a single step, and substituting in our definition for d gives

$$u_{k+1} = \left[I - (P^a + P^{fe} - P^{fe}P^a)\right] u_k + (P^a + P^{fe} - P^{fe}P^a)u_g^a + P^{fe}d. \quad (3.3)$$

Now subtract u_g^a from both sides to give

$$e_{k+1}^a = \left[I - (P^a + P^{fe} - P^{fe}P^a)\right] e_k^a + P^{fe}d. \quad (3.4)$$

The rightmost term arises due to the local-nonlocal interface at the coupling boundary. Let us suppose that the iteration operator has the eigendecomposition $V\Lambda V^{-1}$. Upon substitution, we have

$$e_{k+1}^a = V\Lambda^{k+1}V^{-1}e_0^a + \sum_{i=0}^{k} V\Lambda^i V^{-1}\left(P^{fe}d\right). \quad (3.5)$$

Let σ be the spectral radius of Λ, and let $\kappa(V) \equiv \|V\|\left\|V^{-1}\right\|$ denote the condition number of the eigenvector matrix V, where $\|\cdot\|$ denotes the 2-norm. Taking norms, we have

$$\left\|e_{k+1}^a\right\| \leq \kappa(V)\left\|e_0^a\right\|\sigma^{k+1} + \kappa(V)\left\|P^{fe}d\right\|\sum_{i=0}^{k}\sigma^i \quad (3.6)$$

$$= \kappa(V)\left\|e_0^a\right\|\sigma^{k+1} + \kappa(V)\left\|P^{fe}d\right\|\frac{1-\sigma^{k+1}}{1-\sigma}. \quad (3.7)$$

With the preceding equation, we have just proved the following theorem.

THEOREM 3.1. *Assume $\sigma \neq 1$. The norm of the error with respect to the global atomistic model at iteration $k+1$ of Algorithm 1 can be bound above as*

$$\left\|e_{k+1}^a\right\| \leq \sigma^{k+1}\kappa(V)\left(\left\|e_0^a\right\| - \frac{\left\|P^{fe}d\right\|}{1-\sigma}\right) + \frac{\kappa(V)}{1-\sigma}\left\|P^{fe}d\right\|. \quad (3.8)$$

If $0 < \sigma < 1$, then in the limit as $k \to \infty$, the first term on the right-hand side disappears, and the second is independent of k. Further, σ determines the convergence rate. So, with respect to the global atomistic solution, the (nonconvergent) rightmost term bounds our error. Note that if σ decreases with increasing overlap, we expect faster convergence of our iterative method, and a smaller rightmost term, both of which are incentive to increase the overlap.

We analyze these two terms separately.

3.1. The convergent term. To analyze the convergence rate we must determine σ, which we can do by considering the block structure of the iteration operator. We utilize analysis similar to that of Bjorstad [3]. We begin by writing out the global stiffness matrices for the atomistic and finite element models, where the block struc-

ture of the these matrices indicates the subdomain connectivity:

$$K_g^a = \begin{bmatrix} K_{1,1}^a & 0 & 0 & K_{1,4}^a & 0 \\ 0 & K_{2,2}^a & 0 & 0 & K_{2,5}^a \\ 0 & 0 & K_{3,3}^a & K_{3,4}^a & K_{3,5}^a \\ K_{1,4}^{a^T} & 0 & K_{3,4}^{a^T} & K_{4,4}^a & 0 \\ 0 & K_{2,5}^{a^T} & K_{3,5}^{a^T} & 0 & K_{5,5}^a \end{bmatrix}, \tag{3.9}$$

$$K_g^{fe} = \begin{bmatrix} K_{1,1}^{fe} & 0 & 0 & K_{1,4}^{fe} & 0 \\ 0 & K_{2,2}^{fe} & 0 & 0 & K_{2,5}^{fe} \\ 0 & 0 & K_{3,3}^{fe} & K_{3,4}^{fe} & K_{3,5}^{fe} \\ K_{1,4}^{fe^T} & 0 & K_{3,4}^{fe^T} & K_{4,4}^{fe} & 0 \\ 0 & K_{2,5}^{fe^T} & K_{3,5}^{fe^T} & 0 & K_{5,5}^{fe} \end{bmatrix}. \tag{3.10}$$

Before writing down the projectors we define specific Schur complement operators that will occur frequently.

$$S_4^a = K_{4,4}^a - K_{1,4}^{a^T}(K_{1,1}^a)^{-1}K_{1,4}^a - K_{3,4}^{a^T}(K_{3,4}^a)^{-1}K_{3,4}^a \tag{3.11}$$

$$S_5^{fe} = K_{5,5}^{fe} - K_{2,5}^{fe^T}(K_{2,2}^{fe})^{-1}K_{2,5}^{fe} - K_{3,5}^{fe^T}(K_{3,3}^{fe})^{-1}K_{3,5}^{fe}. \tag{3.12}$$

Applying the definition of the projectors, we see that they take the form

$$P^a \equiv R_2^T(K^{fe})^{-1}R_2K^{fe} = \begin{bmatrix} I & 0 & 0 & 0 & P_{1,5}^a \\ 0 & 0 & 0 & 0 & 0 \\ 0 & 0 & I & 0 & P_{3,5}^a \\ 0 & 0 & 0 & I & P_{4,5}^a \\ 0 & 0 & 0 & 0 & 0 \end{bmatrix}, \tag{3.13}$$

$$P^{fe} \equiv R_1^T(K^a)^{-1}R_1K^a = \begin{bmatrix} 0 & 0 & 0 & 0 & 0 \\ 0 & I & 0 & P_{2,4}^{fe} & 0 \\ 0 & 0 & I & P_{3,4}^{fe} & 0 \\ 0 & 0 & 0 & 0 & 0 \\ 0 & 0 & 0 & P_{5,4}^{fe} & I \end{bmatrix}, \tag{3.14}$$

where the block submatrices take the form

$$\begin{aligned} P_{1,5}^a &= (K_{1,1}^a)^{-1}K_{1,4}^a(S_4^a)^{-1}K_{3,4}^{a^T}(K_{3,3}^a)^{-1}K_{3,5}^a, \\ P_{3,5}^a &= (K_{3,3}^a)^{-1}\left(K_{3,5}^a + K_{3,4}^a(S_4^a)^{-1}K_{3,4}^{a^T}(K_{3,3}^a)^{-1}K_{3,5}^a\right), \\ P_{4,5}^a &= -(S_4^a)^{-1}K_{3,4}^{a^T}(K_{3,3}^a)^{-1}K_{3,5}^a, \\ P_{2,4}^{fe} &= (K_{2,2}^{fe})^{-1}K_{2,5}^{fe}(S_5^{fe})^{-1}K_{3,5}^{fe^T}(K_{3,3}^{fe})^{-1}K_{3,4}^{fe}, \\ P_{3,4}^{fe} &= (K_{3,3}^{fe})^{-1}\left(K_{3,4}^{fe} + K_{3,5}^{fe}(S_5^{fe})^{-1}K_{3,5}^{fe^T}(K_{3,3}^{fe})^{-1}K_{3,4}^{fe}\right), \\ P_{5,4}^{fe} &= -(S_5^{fe})^{-1}K_{3,5}^{fe^T}(K_{3,3}^{fe})^{-1}K_{3,4}^{fe}. \end{aligned}$$

We now have that

$$P^a + P^{fe} - P^{fe}P^a = \begin{bmatrix} I & 0 & 0 & 0 & P_{1,5}^a \\ 0 & I & 0 & 0 & -P_{2,4}^{fe}P_{4,5}^a \\ 0 & 0 & I & 0 & -P_{3,4}^{fe}P_{4,5}^a \\ 0 & 0 & 0 & I & P_{4,5}^a \\ 0 & 0 & 0 & 0 & I - P_{5,4}^{fe}P_{4,5}^a \end{bmatrix}.$$

Clearly, the iteration operator $I - P^a + P^{fe} - P^{fe}P^a$ is a block upper-triangular matrix with zero blocks on all but the last entry of the diagonal, which is equal to $P^{fe}_{5,4}P^a_{4,5}$. Thus, we have that σ is the maximum magnitude eigenvalue of $P^{fe}_{5,4}P^a_{4,5}$.

3.2. The nonconvergent term. To analyze the behavior of the rightmost term in our bound, we must consider $\left\|P^{fe}d\right\|$. As we have broken our global domain into five subdomains $\Omega_1, \ldots, \Omega_5$, we also break the vector d into five subvectors, such that $d = \left[d_1^T, d_2^T, d_3^T, d_4^T, d_5^T\right]^T$. Here, the structure of P^{fe} is important. P^{fe} operates only on the portions of the global problem that are in the finite element domain Ω^{fe}, and ignores the purely atomistic subdomain Ω_1. Specifically,

$$\begin{aligned}\left\|P^{fe}d\right\|_2^2 = \left\|d_2 + P^{fe}_{2,4}d_4\right\|^2 + \left\|d_3 + P^{fe}_{3,4}d_4\right\|^2 + \left\|P^{fe}_{5,4}d_4 + d_5\right\|^2 \\ \sim \|d_2\|^2 + \|d_3\|^2 + \|d_4\|^2 + \|d_5\|^2 .\end{aligned}$$

We see that the value of d_1 (the difference of the atomistic and continuum solutions *in the purely atomistic subdomain* Ω_1) does not appear. In general, the domain Ω_1 was chosen to be a purely atomistic in the coupled model because a finite element solution in this domain does not produce acceptable results. Thus, we expect the finite element solution and the atomistic solution in the domain Ω_1 to be different. That is, we expect that $d_1 \neq 0$. Fortunately, this does not prohibit our coupled model from recovering the global atomistic solution. We will see in the next section that the error of the converged solution depends not only on the location but also the size of the pad region.

We can easily identify one situation when we expect $\left\|P^{fe}d\right\| = 0$. In particular, we will have $d_i = 0$, $i = 2, \ldots, 5$ if the atomistic and finite element displacement are identical in domains $\Omega_2, \ldots \Omega_5$. This means that the displacement of the macroscopic model (the finite element model) exactly matches the displacement of the microscopic model (the atomistic model) in the domain Ω^{fe}.

REMARK 3.2. *We expect that* $\left\|P^{fe}d\right\| = 0$ *if the deformation in* Ω^{fe} *is a Cauchy-Born deformation, regardless of the deformation in* Ω_1.

In particular, our linear spring model and our choice of finite element shape functions can both reproduce exactly a constant strain solution under an applied constant stress. In finite element parlance, recovering a constant strain solution given an applied constant stress satisfies a *patch test* [33]. We consider this specific example in section 4.2.

4. Numerical Results. The results in the previous section are general in that they do not depend on the number of dimensions of the model, the shape of the atomistic or finite element subdomains, the finite element discretization, or the specifics of the mass-spring model used in the atomistic subdomain. To demonstrate theoretical results, we will propose a specific one dimensional model, and then analyze it.

4.1. A One Dimensional Overlapping Schwarz Model. Here we propose one-dimensional atomistic, finite element, and coupled models based on the one dimensional models described in [8]. Our global atomistic model is represented by a mass-spring system of 105 atoms with lattice constant α where nearest-neighbor atoms are bonded by a spring of stiffness k_1^a and second-neighbor atoms are bonded by a spring of stiffness k_2^a. (Hence, we have a second-nearest neighbor model with $r = 2$). We number the atoms/nodes from left to right, $1, \ldots, 105$. The two leftmost and two rightmost atoms will be held fixed in all cases. Our global finite element model will consist of 104 truss elements, where the two rightmost and two leftmost nodes are

held Dirichlet. In particular, the fixed atom positions of the atomistic model and fixed displacements of the Dirichlet finite element nodes will be set consistently. Each finite element has an equilibrium length α and a Young's modulus such that the effective spring constant is k^{fe}. Under a uniform deformation field, we would like the strain energies of the two models to match, so we fix $k^{fe} = 4k_1^a + k_2^a$. We construct a coupled model by overlapping an atomistic subdomain with a finite element subdomain, as discussed in section 2. Domain Ω_1 denotes a purely atomistic subdomain, domain Ω_2 a purely finite element subdomain, and domains Ω_3, Ω_4, and Ω_5 the subdomains in the overlap region. When solving for new atom positions in the atomistic subdomain Ω^a, we hold the atoms in domain Ω_5 fixed. Since $r = 2$ for our model, we have only two atoms in domain Ω_4. In general, the number of fixed-displacement atoms must be large enough to avoid the appearance of surface effects in the overlap region. The subdomain boundaries here are artificial, and surface effects are nonphysical. Likewise, when solving for new node positions in the finite element subdomain Ω^{fe}, we hold the nodes in domain Ω_4 fixed. As our finite element shape functions have only local support, we require only one Dirichlet node in subdomain Ω_4. However, to avoid coupling between domains Ω_1 and Ω_3 in the atomistic model, we instead define Ω_4 to include two atoms/nodes. The region around the interface is depicted in Figure 4.1.

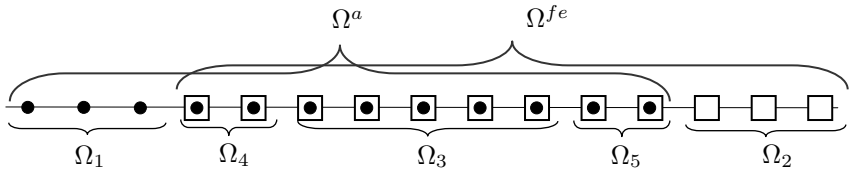

FIG. 4.1. *The overlap region for the 1D coupled model consists of domains Ω_4, Ω_3, and Ω_5. In this figure, circles represent atoms and squares finite element nodes. When solving in domain Ω^a, the atoms in domain Ω_5 are held fixed. When solving in domain Ω^{fe}, the finite element nodes in domain Ω_4 are held fixed.*

To study how overlap affects convergence, we define an overlap parameter δ, as shown in Figure 4.2. Let the middle atom/node in the coupled model be denoted as I. An overlap of $\delta = 1$ specifies one overlapping atom/node to the left and right of atom/node I. An overlap of $\delta = 2$ specifies two overlapping atoms/nodes to the left and right of atom/node I, etc. Recall that we are considering an atomistic model with $r = 2$ (nearest-neighbor and second-nearest-neighbor coupling). As a result, we will only consider configurations where domain Ω_3 has at least two atoms in order to avoid direct coupling between domains Ω_4 and Ω_5. This means we will only consider overlap values of $\delta \geq 2$.

Referring to Figure 2.2, we note that the particular 1D mass-spring model we use can easily be shown to be a finite difference discretization with a particular stencil of the equation

$$-\frac{d}{dx}\left(k^{fe}\frac{du}{dx}\right) = f.$$

In the limit as the lattice constant goes to zero, this PDE is recovered. Further, our finite element model is a finite element discretization of the same PDE, and likewise recovers this PDE in the limit as the mesh spacing goes to zero.

4.2. Constant Strain. We first examine the ability of the coupled model to reproduce a constant-strain solution. We begin by setting two leftmost atoms and the two rightmost finite element nodes to have a position/displacement consistent

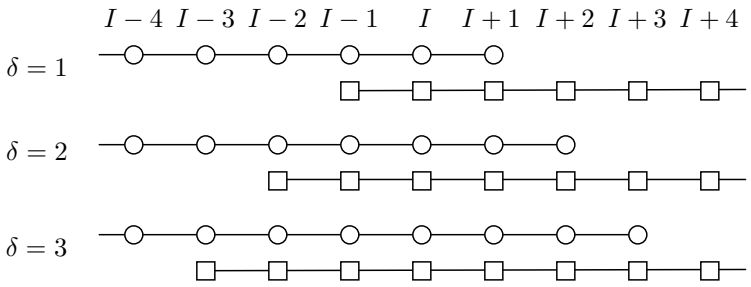

FIG. 4.2. *The overlap region for the 1D coupled model for various values of overlap δ. Let circles denote atoms and squares denote finite element nodes, with the middle atom/node as I.*

δ	Convergence Rate	σ	Num. Iterations	$\|u - u_g^a\|$	2^{nd} term from (3.8)	$\|P^{fe}d\|$
2	.9195	.9195	287	1.09×10^{-12}	3.11×10^{1}	4.16×10^{-17}
3	.8501	.8501	153	5.37×10^{-13}	1.79×10^{-2}	4.48×10^{-17}
4	.7859	.7859	106	2.90×10^{-13}	7.82×10^{-4}	4.82×10^{-17}
5	.7264	.7264	93	2.20×10^{-13}	1.69×10^{-5}	4.57×10^{-17}

TABLE 4.1
Data for section 4.2: constant strain.

with a constant strain of 0.01. We also fix the position of the leftmost atom at the origin. We solved the coupled model using algorithm 1 with a convergence tolerance of $\varepsilon = 1.0 \times 10^{-13}$ for several values of δ. Convergence data is shown in Table 4.1. A plot of the computed strain solution for the coupled model is shown in Figure 4.3(a), showing a constant strain throughout the domain, including the overlap region. For these boundary conditions, $\|d\| = 9.2 \times 10^{-17}$. In particular, this means $\|d_2\| = \|d_3\| = \|d_4\| = \|d_5\| = 0$ to within machine precision (see the last column of Table 4.1) which is precisely the case where the coupled model can recover the global atomistic solution. The bound (3.8) is plotted in Figure 4.3(b).

One item of note is that $\kappa(V)$ (the condition number of the eigenvector matrix) is quite large. The iteration operator is nonsymmetric, so this is not unexpected. In this example, the bound (3.8) is useful in that it predicts when the error can be zero, even though it is not numerically tight. One alternative approach is to modify Algorithm 1 to a symmetric alternating Schwarz algorithm. In this algorithm, the iteration operator becomes symmetric, thus forcing its eigenvector matrix to have a condition number of one. Although producing a tighter bound, this symmetric version of the algorithm is less useful in practice as it is more expensive per iteration.

4.3. A Point Force in the Atomistic Subdomain. In this section, we consider applying a point force to atom 25 in the atomistic subdomain, and study how well the global atomistic solution is recovered by the coupled model.

To set the positions of the fixed atoms and nodes in the finite element model, we proceed by attempting to match the local strains at the ends with those of a global finite element model. We first solve the global finite element problem setting the four Dirichlet nodes such that a constant strain of 0.01 results in the absence of external forces. We then fix the two leftmost atom and two rightmost finite element node positions to match those of the global finite element model. Without loss of generality, the leftmost atom is always held fixed at the origin.

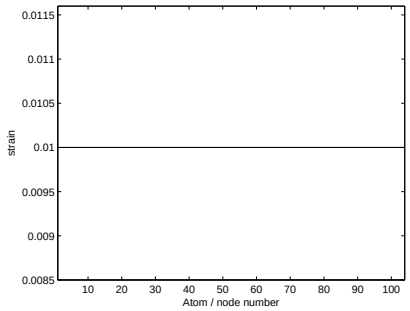

(a) Computed strain for global atomistic model and coupled model. (Curves are identical).

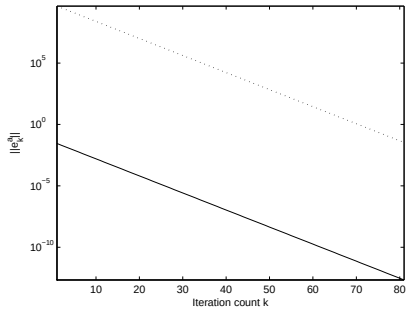

(b) Convergence curve (solid line) and bound (3.8) (dashed line) for $\delta = 5$.

FIG. 4.3. *Plots for section 4.2: constant strain.*

δ	Convergence Rate	σ	Num. Iterations	$\|u - u_g^a\|$	2^{nd} term from (3.8)	$\|P^{fe}d\|$
2	.9195	.9195	288	1.12×10^{-12}	4.24×10^{1}	5.65×10^{-17}
3	.8501	.8501	154	5.06×10^{-13}	2.49×10^{-2}	2.49×10^{-17}
4	.7859	.7859	106	3.20×10^{-13}	9.69×10^{-4}	9.69×10^{-17}
5	.7264	.7264	81	2.42×10^{-13}	2.11×10^{-5}	2.11×10^{-17}

TABLE 4.2
Data for section 4.3: point force in pure atomistic domain Ω_1.

We solved the coupled model using algorithm 1 with a convergence tolerance of $\varepsilon = 1.0 \times 10^{-13}$ for several values of δ. Convergence data is shown in Table 4.2. A plot of the computed strain for the coupled model is shown in Figure 4.4(a), showing a jump in the strain at the point of application of the force. The bound (3.8) is plotted in Figure 4.4(b).

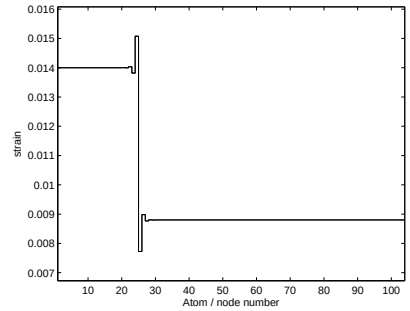

(a) Computed strain for global atomistic model and coupled model. (Curves are identical).

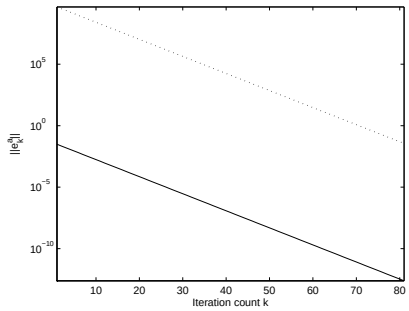

(b) Convergence curve (solid line) and bound (3.8) (dashed line) for $\delta = 5$.

FIG. 4.4. *Plots for section 4.3: point force in pure atomistic domain Ω_1.*

For this case, $\|d\| \approx 9.1 \times 10^{-6}$. Although $\|d_1\| \neq 0$, we have $\|d_2\| = \|d_3\| = \|d_4\| = \|d_5\| = 0$ to within machine precision (see the last column of Table 4.2), allowing the coupled model to again recover the global atomistic solution. That

δ	Convergence Rate	σ	Num. Iterations	$\|u - u_g^a\|$	2^{nd} term from (3.8)	$\|P^{fe}d\|$
2	.9195	.9195	290	1.77×10^{-5}	8.92×10^{12}	1.19×10^{-5}
3	.8501	.8501	154	1.66×10^{-6}	3.59×10^{9}	9.00×10^{-6}
4	.7859	.7859	106	2.02×10^{-7}	1.48×10^{8}	9.13×10^{-6}
5	.7264	.7264	82	2.78×10^{-8}	3.36×10^{6}	9.10×10^{-6}

TABLE 4.3
Data for section 4.4: point force in overlap domain Ω_3.

is, the atomistic and finite element models disagree only in Ω_1, a domain we have designated to be a purely atomistic domain, and so our coupled model will recover the global atomistic solution.

4.4. A Point Force in the Overlap Region. In this section, we apply a point force to atom I in the coupled model–essentially the worst location to apply a force, and study how well the global atomistic solution is recovered by the coupled model.

We set the fixed-displacement atoms and nodes as in the previous section. We then solved the coupled model using algorithm 1 with a convergence tolerance of $\varepsilon = 1.0 \times 10^{-13}$ for several values of δ. Convergence data is shown in Table 4.3. A plot of the computed strain near the pad region is in Figure 4.5 for several values of δ. Observe that the quality of the solution improves as δ increases, meaning that the error depends not only on the placement of the overlap region (with respect to the location of the point force) but also varies with the size of the overlap. This result is in sharp contrast to convergence results for alternating Schwarz applied to a standard finite element discretization of an elliptic PDE, for example [32, 29]. In this example we have a nonuniform displacement field in the overlap region. Correspondingly, we notice that $\|P^{fe}d\|$ in Table 4.3 does not decrease below a minimum value, and is much larger than $\|P^{fe}d\|$ in Tables 4.1 and 4.2. The nonconvergent term in (3.8) is not small in this example, and so the error in the converged solution is larger, as well.

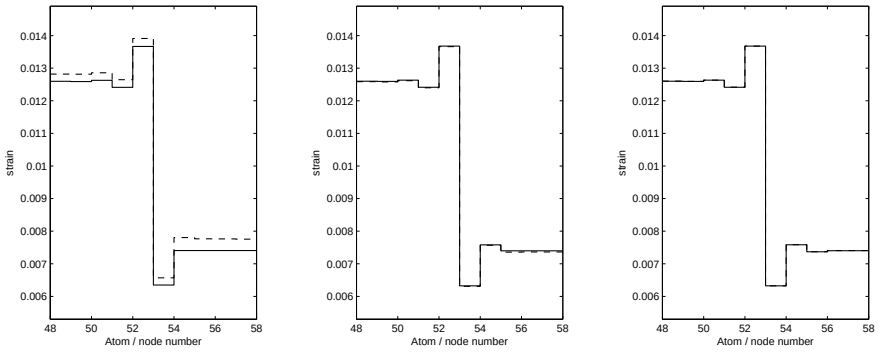

(a) $\delta = 2$ (b) $\delta = 3$ (c) $\delta = 4$

FIG. 4.5. *Plots for section 4.4: point force in overlap domain Ω_3. Computed strains are shown for the global atomistic model (dashed line) and the coupled model (solid line) The $\delta = 5$ strain plot (not shown) is visually indistinguishable from the $\delta = 4$ strain plot.*

δ	Convergence Rate	Num. Iterations	$\|u - u_g^a\|$
2	.9258	241	1.92×10^{-5}
3	.8569	126	1.92×10^{-5}
4	.7930	87	1.92×10^{-5}
5	.7336	67	1.92×10^{-5}

TABLE 4.4

Data for section 4.5: Coupling a Lennard-Jones and finite element model with a point force in pure atomistic domain Ω_1.

4.5. Coupling Lennard-Jones and Finite Element Models. In this section, we couple a one-dimensional Lennard-Jones atomistic model [18] with our finite element model, and study how well the global atomistic solution is recovered by the coupled model. The well-known Lennard-Jones potential can be written as

$$U_{ij} = 4\epsilon \left(\left(\frac{s}{r_{ij}} \right)^{12} - \left(\frac{s}{r_{ij}} \right)^{6} \right), \tag{4.1}$$

where $r_{ij} = |x_i - x_j|$ is the distance between two atoms. For this model, we fixed $\epsilon = 1/4$, $s = 2\sqrt[3]{2}$, and set a lattice constant $\alpha = \sqrt[6]{2}s$. Additionally, we set a cutoff of $2.5s$.

To match the Lennard-Jones with our finite element model, we linearized the Lennard-Jones force and set the stiffness k^{fe} to match the linearized Lennard-Jones force, so that both models will agree to first order, and hence only for small deformations.

We set the fixed-displacement atoms and nodes as in the previous section and apply a point force to atom 25, just as in section 4.3. We then solve the coupled model using algorithm 1 with a convergence tolerance of $\varepsilon = 1.0 \times 10^{-13}$ for several values of δ. Convergence data is shown in Table 4.4. We observe an increase in convergence rate with increasing δ, just as when we coupled with a mass-spring model. We also observe that the absolute error is essentially constant with δ, which we expect, given that the point force is applied far from the overlap region.

5. Conclusions. We have demonstrated that a broad class of atomistic/continuum coupling algorithms may be placed within the framework of the alternating Schwarz domain decomposition algorithm. For the specific case of coupling a mass-spring network with a finite element model, we have developed a convergence bound and also shown when the coupled model will recover exactly the solution of the mass-spring system. In particular, we identified convergent and nonconvergent parts of the error, and demonstrated experimentally that the convergence rate increased with the size of the overlap. In contract to alternating Schwarz applied to a finite element discretization, we showed that the error can depend not only on the size but also the placement of the overlap region with respect to external applied forces. In particular, based on our experiments, it is clear the overlap region should be placed sufficiently far away from regions where the continuum model is not valid.

In closing, we observe that many improvements have been made to the classical alternating Schwarz domain decomposition algorithm, including acceleration by modification of the transmission conditions between subdomains [13]. A next logical step is to extend these acceleration techniques to the atomistic/continuum setting.

Acknowledgements. The authors acknowledge funding by the DOE Office of Science Advanced Scientific Computing Research Program, and by the Sandia Laboratory Directed Research and Development program. The authors also acknowledge helpful comments from Jacob Fish and Mark Sheppard.

REFERENCES

[1] M. Arndt and M. Griebel, *Derivation of higher order gradient continuum models from atomistic models for crystalline solids.*, Multiscale Model. Simul., 4 (2005), pp. 531–562.
[2] M. Berezhnyy and L. Berlyand, *Continuum limit for three-dimensional mass-spring networks and discrete Korn's inequality*, J. Mech. Phys. Solids, 54 (2006), pp. 635–669.
[3] P. E. Bjørstad, *Multiplicative and additive Schwarz' methods: Convergence in the 2-domain case*, in Proceedings of the Second International Symposium on Domain Decomposition Methods, Los Angeles, California, January 14-16, T. Chan, R. Glowinski, J. Priaux, and O. Widlund, eds., SIAM, 1988.
[4] X. Blanc, C. L. Bris, and F. Legoll, *Analysis of a prototypical multiscale method coupling atomistic and continuum mechanics*, Math. Model. Num. Anal., 39 (2005), pp. 797–826.
[5] X. Blanc, C. L. Bris, and P.-L. Lions, *From molecular models to continuum mechanics*, Archive for Rational Mechanics and Analysis, 164 (2002), pp. 341–381.
[6] M. Born and K. Huang, *Dynamical Theory of Crystal Lattices*, Clarendon Press, Oxford, 1954.
[7] R. D. Cook, D. S. Malkus, M. E. Plesha, and R. J. Witt, *Concepts and Applications of Finite Element Analysis*, John Wiley & Sons, New York, 4th ed., 2002.
[8] W. Curtin and R. Miller, *Atomistic/continuum coupling methods in multi-scale materials modeling*, Modeling and Simulation in Materials Science and Engineering, 11 (2003), pp. R33–R68.
[9] W. E and Z. Huang, *A dynamic atomistic-continuum method for the simulation of crystalline materials*, Journal of Computational Physics, 182 (2002), pp. 234–261.
[10] W. E and P. B. Ming, *Analysis of the local quasicontinuum method*, in Frontiers and Prospects of Contemporary Applied Mathematics, T. Li and P. Zhang, eds., Higher Education Press, World Scientific, 2005, pp. 18–32.
[11] J. L. Ericksen, *The Cauchy and Born hypotheses for crystals*, in Phase Transformations and Material Instabilities in Solids, Academic Press, 1984.
[12] J. Fish, *Bridging the scales in nano engineering and science*, J. Nanopart. Res., (2006). In print.
[13] M. Gander, *Optimized Schwarz methods*, SIAM J. Num. Anal., 44 (2006), pp. 699–731.
[14] N. G. Hadjiconstantinou, *Hybrid atomistic-continuum formulations and the moving contact-line problem*, Journal of Computational Physics, 154 (1999), pp. 245–265.
[15] ———, *Discussion of recent developments in hybrid atomistic-continuum methods for multiscale hydrodynamics*, Bulletin of the Polish Academy of Sciences, 53 (2005), pp. 335–342.
[16] J. Knap and M. Ortiz, *An analysis of the quasicontinuum method*, Journal of the Mechanics and Physics of Solids, 49 (2001), pp. 1899–1923.
[17] S. Kohlhoff, P. Gumbsch, and H. F. Fischmeister, *Crack propagation in b.c.c. crystals studied with a combined finite-element and atomistic model*, Philosophical Magazine A, 64 (1991), pp. 851–878.
[18] J. E. Lennard-Jones, *Cohesion*, Proceedings of the Physical Society, 43 (1931), pp. 461–482.
[19] J. Li, D. Liao, and S. Yip, *Nearly exact solution for coupled continuum/md fluid simulation*, Phys. Rev. E, 57 (1998), pp. 7259–7267.
[20] ———, *Imposing field boundary conditions in md simulation of fluids: optimal particle controller and buffer zone feedback*, in Mater. Res. Soc. Symp. Proc., T. D. de la Rubia, T. Kaxiras, V. Bulatov, N. Ghoniem, and R. Phillips, eds., vol. 538, 1999, pp. 473–8.
[21] ———, *Nearly exact solution for coupled continuum/md fluid simulation*, Journal of Computer-Aided Materials Design, 6 (1999), pp. 95–102.
[22] P. Lin, *Theoretical and numerical analysis for the quasi-continuum approximation of a material particle model*, Mathematics of Computation, 72 (2003), pp. 657–675.
[23] ———, *Convergence analysis of a quasi-continuum approximation for a two-dimensional material*, SIAM J Numer. Anal., (2005). To appear.
[24] G. Lu and E. Kaxiras, *Overview of multiscale simulations of materials*, in Handbook of Theoretical and Computational Nanotechnology, M. Rieth and W. Schommers, eds., vol. X, American Scientific Publishers, 2005, ch. 22, pp. 1–33.

[25] R. E. Miller and E. B. Tadmor, *The quasicontinuum method: Overview, applications, and current directions*, Journal of Computer-Aided Materials Design, 9 (2002), pp. 203–239.
[26] X. B. Nie, S. Y. Chen, W. E, and M. O. Robbins, *A continuum and molecular dynamics hybrid method for micro- and nano-fluid flow*, J. Fluid Mech., 500 (2004), pp. 55–64.
[27] X. B. Nie, S. Y. Chen, and M. O. Robbins, *Hybrid continuum-atomistic simulation of singular corner flow*, Physics of Fluids, 15 (2004), pp. 3579–3591.
[28] H. S. Park and W. K. Liu, *An introduction and tutorial of multiple-scale analysis in solids*, Comput. Methods Appl. Mech. Engrg., 193 (2004), pp. 1733–1772.
[29] A. Quarteroni and A. Valli, *Domain Decomposition Methods for Partial Differential Equations*, Oxford University Press, Oxford, 1999.
[30] H. A. Schwarz, *Gesammelete Mathematische Abhandlungen*, vol. 2, Springer, Berlin, 1890, pp. 133–143. First published in Vierteljahrsschrift der Naturforschenden Gesellschaft in Zürich, volume 15, 1870, pp. 272–286.
[31] V. B. Shenoy, R. Miller, E. B. Tadmor, D. Rodney, R. Phillips, and M. Ortiz, *An adaptive finite element approach to atomic-scale mechanics – the quasicontinuum method*, Journal of the Mechanics and Physics of Solids, 47 (1999), pp. 611–642.
[32] B. Smith, P. E. Bjørstad, and W. Gropp, *Domain Decomposition: Parallel Multilevel Methods for Elliptic Partial Differential Equations*, Cambridge University Press, 1999.
[33] G. Strang and G. J. Fix, *An Analysis of the Finite Element Method*, Series in Automatic Computation, Prentice-Hall, 1973.
[34] E. B. Tadmor, M. Ortiz, and R. Phillips, *Quasicontinuum analysis of defects in solids*, Philosophical Magazine A, 73 (1996), pp. 1529–1563.
[35] Z. Tang and N. R. Aluru, *A combined atomistic/continuum analysis of nanoelectromechanical systems*, in IEEE-NANO 2003, Third IEEE Conference on Nanotechnology, vol. 2, San Francisco, Aug. 12-14 2003, IEEE Press, pp. 191–194.
[36] D. D. Vvedensky, *Multiscale modelling of nanostructures*, J. Phys. Condens. Matter, 16 (2004), pp. R1537–R1576.
[37] T. Werder, J. H. Walther, and P. Koumoutsakos, *Hybrid atomistic–continuum method for the simulation of dense fluid flows*, Journal of Computational Physics, 205 (2005), pp. 373–290.
[38] H. S. Wijesinghe and N. G. Hadjiconstantinou, *Discussion of hybrid atomistic-continuum methods for multiscale hydrodynamics*, International Journal for Multiscale Computational Engineering, 2 (2004), pp. 189–202.